Dynamic behavior of reinforced concrete beams under varying rates of concentrated loading

Satadru Das Adhikarya, Bing Li [a,,] Kazunori Fujikake [b]*

[a] *School of Civil and Environmental Engineering, Nanyang Technological University, Singapore 639798, Singapore*
[b] *Department of Civil and Environmental Engineering, National Defense Academy, Yokosuka 239 8686, Japan*
[*] *Corresponding author. Tel.: +65 67905292. E-mail address: cbli@ntu.edu.sg (B. Li)*

Abstract

The behavior under varying rates of concentrated loading of reinforced concrete (RC) beams was studied, aimed at attaining a better understanding of the effects of loading rates on RC beams. The test program was successful in providing a substantial volume of test data including load vs. mid-span displacement, crack profiles, strain at the mid-point of longitudinal tensile reinforcements and acceleration at several locations along the specimens. Peak load, stiffness, absorption energy and strain rate were found to increase with the enhancement of loading rates. LS-DYNA, an explicit finite element program widely used for three-dimensional nonlinear transient analysis of structures, was employed in this study to provide numerical simulations of RC beams under varying loading rates. Three-dimensional finite element (FE) models of RC beams have been described and verified with the experimental results, followed by a parametric study to investigate the influence of the longitudinal reinforcement ratio, the transverse reinforcement ratio and the shear span to effective depth ratio. Empirical equations are proposed in terms of various parameters to predict the Dynamic Increase Factor (DIF) of maximum resistance of RC beams under varying loading rates.

Keywords: RC beam; Loading rate; Strain rate; DIF; Numerical simulation

1. Introduction

During service life of RC structures, they may be subjected to various types of dynamic loading in the form of earthquakes, blasts or impact. In all these cases, it is of fundamental importance to understand the effect of loading rate on structures. Despite this, current knowledge on the behavior of reinforced concrete (RC) structures subjected to varying rates of concentrated loading is still considered to be in its infancy. In this article, loading rates at the mid-point of RC beam constitute a wide spectrum ranging from 4×10^{-4} m/s to 2 m/s. Corresponding peak strain rates at the mid-span of longitudinal tensile reinforcement are generated from these loading rates, ranging from 10^{-4} to 10/s respectively.

RC structures are composite constructs, constituting plain concrete and steel reinforcements. Therefore, the effect of loading rate on a reinforced concrete structural element is influenced by the loading rate sensitivity of the mechanical characteristics of the materials involved. The strength characteristics of plain concrete and reinforcement are known to be enhanced due to increasing loading rates [1]. However, plain concrete exhibits an increasingly brittle nature with an increasing loading rate. Therefore, the resulting response of reinforced concrete structures to varying rates of concentrated loading depends on both the loading rate (i.e., duration of loading) and the rate sensitivity of the materials used.

Compared to impact/impulsive loading [2-6], less information is available in the literature on RC beams under varying rates of concentrated loading at their mid-span in displacement control. Seven pairs of singly reinforced concrete (without transverse reinforcements) beams were tested by Kulkarni and Shah [7]. For each pair, one beam was tested at a "static" rate (piston velocity 0.0000071 m/s) and the other at a "high" rate (piston velocity 0.38 m/s). Fujikake et al. [8] also carried out the testing of three pairs of doubly reinforced concrete (with shear reinforcements) beams under displacement control. For each pair, one beam was tested at a "static" rate (0.0005 m/s) and the other at a "high" rate (2 m/s). Fujikake et al. considered a much higher piston velocity for high rates as compared to Kulkarni and Shah. With the aim of obtaining information in this area, an experimental program was undertaken for RC beams subjected to a wide range of loading rates (Static: 4×10^{-4}, Low: 4×10^{-2}, Medium: 0.4 and High: 2 m/s). This paper summarizes the details of the test program; including specimen properties, test setup, instrumentations and test procedures. The test results and major observations are presented and discussed. FE analysis utilizing LS-DYNA [9] is performed for the numerical simulation of the RC beams under varying rates of concentrated loading. The FE model is verified with the experimental (both from available and present study) results. This is followed by an extensive parametric study to investigate the influence of the longitudinal reinforcement ratio, the transverse reinforcement ratio and the shear span to effective depth ratio. Empirical equations are proposed in terms of various parameters to predict the dynamic increase factor (DIF) of maximum resistance of RC beams (with and without transverse reinforcements) under varying loading rates. The dynamic increase factor (DIF) was calculated as a ratio of maximum resistance of RC beam at any loading rate (i.e. low, medium and high) to the corresponding static maximum resistance at a loading rate of 4×10^{-4} m/s.

2. Review of past experimental data

As mentioned earlier, few experiments (Kulkarni & Shah, Fujikake et al. and Mutsuyoshi & Machida) have been carried out to date to investigate the response of RC beams under varying rates of concentrated loading at their mid-span. The tendency toward brittle shear failure of reinforced concrete beams at a higher loading rate was reported by Mutsuyoshi and Machida [10] although the beams were flexure-critical under static loading. As a result, the RC beams exhibited reduced ductility capacity from a different mode of failure (transition in failure mode from flexure to shear). The nature of loading (duration of high loading rate, in a few milliseconds) and the rate sensitivity of the materials (concrete and steel reinforcing bars) used would be the main reasons for this

change in the failure mode of RC beams under high loading rates. There was a significant amount of inertial forces when the beams were subjected to high dynamic loading within a very short time interval. This significant amount of inertial forces forced the beam to take a deflected shape that was different from the static deflected shape. This different deflected shape was responsible for a higher maximum shear force and lower maximum moment in RC beams under high loading rate. This demonstrated a tendency toward shear failure under high loading rate. Singly reinforced concrete beams without shear reinforcements were tested by Kulkarni and Shah. All the beams tested were relatively close to the shear failure regime. The deflected shape of RC beams was almost identical at the two rates. Peak load and energy absorption capacity were found to increase with increasing loading rate. The load vs. mid-span deflection curves of the beams failing in flexure under high rate did not show a sharp "yield point" or "yield plateau". The reason for this was believed to be the extremely localized yielding of reinforced bars due to enhanced bond properties at high loading rates. The total number of cracks was reduced significantly at the high rate. However, the final failure mode shifted from shear failure at static loading to flexure failure at the high rate for three pairs of reinforced concrete beams. This phenomenon runs counter to the brittle transition in the mode of failure under high loading rates reported by Mutsuyoshi and Machida. Kulkarni & Shah proposed that this apparent contradiction could be explained on the basis of the rate sensitivity of the different grades of steel used in their study. From Fig. 1, it is clear that the flexural strength of RC beams used by Mutsuyoshi and Machida increased at a much higher rate than the shear strength, indicating an increased tendency toward shear failure at high rates. However, the converse is true for RC beams used by Kulkarni & Shah and Fujikake et al. carried out the testing of doubly reinforced concrete beams (with shear reinforcements) under static and high loading rates. All beams were designed as under-reinforced and with a shear to bending resistance ratio greater than one. The influence of dynamic vibration was observed in the load vs. mid-span deflection relationships at high loading rate. All the specimens exhibited flexure failure under both static and high rates of concentrated loading at their mid-span. The ultimate load carrying capacity of the RC beams increased with the increment of longitudinal tensile reinforcements for both static (5×10^{-4} m/s) and high loading rates (2 m/s). Fig. 2 illustrates the dynamic increase factor of RC beams tested by Kulkarni and Shah and Fujikake et al. The average value of dynamic increase factors (i.e., the ratio of dynamic to static strength) of specimens were observed to be 1.17 and 1.25 for the beams tested by Kulkarni & Shah and Fujikake et al. for 0.38 m/s and 2 m/s loading rate respectively.

3. Experimental overview

3.1.Dimensions and static design values of RC beams

The beams (total span length 1700 mm) had rectangular cross-sections of 150 mm width and 250 mm depth. Shear span to effective depth ratio of all the beams was 3.33. The layout of the longitudinal reinforcements, spacing of shear reinforcements and the measuring points (acceleration and strain for steel reinforcing bars) are shown in Fig. 3. Longitudinal reinforcements consisted of four deformed steel bars of D22 mm while D6 deformed bars, were used for shear reinforcements. The specified concrete compressive strength at 28 days was 40 MPa with maximum aggregate size of 20 mm for all

specimens. The yield strengths of D22 and D6 were 371 MPa and 342 MPa, respectively. All the specimens had the same extent (2.4%) of longitudinal reinforcements. 40 mm concrete cover was provided in all the specimens. There was no shear reinforcement in Specimen RC3_S0 whereas 0.12% and 0.56% shear reinforcements were provided in Specimens RC3_S12 and RC3_S56 respectively. Ready mix concrete was used to cast the specimens. The static design parameters for the beams are listed in Table 1, where the static flexural and shear resistances are calculated according to ACI 318-08 [11]. RC3_S56 demonstrated flexure-critical behavior (shear to bending resistance ratio is greater than one) with a ductile response, while RC3_S0 and RC3_S12 were shear-critical with a brittle failure (shear to bending resistance ratio is less than one) mode under monotonically increasing static loads. All specimens were well instrumented to capture the load, displacements, accelerations and steel rebar strains. The instrumentation for this test program included a load cell, strain gauges and accelerometers. A load cell of capacity of 980 kN and measuring frequency of 5 kHz was attached to the actuator to measure the load. 2 mm strain gauges were installed in the mid-span of the longitudinal tensile reinforcements and in the mid-point of the two legs of the transverse reinforcements. Five accelerometers (capacity of 1000 times gravity and resonance frequency more than 70 kHz) were mounted for each test (except static loading) on the specimens to measure the accelerations for low, medium and high rates of concentrated loading. The mid-span deflection of RC beams was measured by laser-type variable displacement transducers (LVDTs) which have a measuring range of 80 mm and sampling rate of 50 kHz. Data from the sensors were collected by a digital data acquisition system which has a sampling rate of 100 Hz, 10 kHz, 100 kHz, and 200 kHz for static, low, medium and high loading rates respectively. The specific locations of the strain gauges and accelerometers are shown in Fig. 3. A steel plate (40 mm thickness) was placed on the top of the beam at loading point to transfer well-distributed force to RC beams. The use of digital photography and high-speed video recording proved to be valuable in providing insights into the cracking patterns and failure modes of the RC beams, particularly the spalling of concrete, and the bending of the longitudinal reinforcing bars.

3.2.Test program

The RC beams used here were designated using two variables: amount of shear reinforcement ratios (0%, 0.12%, and 0.56%) and rate of loading under displacement control [static (S), low (L), medium (M) and high (H)]. There were three types of RC beams, distinguished in terms of shear reinforcement ratios (0%, 0.12% and 0.56%). For each type there were four pairs of specimens subjected to four different loading rates. A schematic diagram of the test setup is shown in Fig. 4. A digitally controlled servo-hydraulic test system was used in this study. The test frame had been designed to be stiff enough. The static test was completed in a few minutes while the low, medium and high rate tests were completed in 1 s, 100 ms and 20 ms respectively.

4. Experimental results and discussions

4.1.Load-midspan deflection curves

The load acting on RC beams was measured by a load cell. Accelerations were measured by the accelerometers placed along the specimens. Inertia force was calculated by considering the linear variation of the accelerations between two adjacent accelerometers. Then, inertia force was eliminated from the measured load by load cell to evaluate the true resistance of the RC beams. Deflection was measured at the mid-span of the reinforced concrete beams. From Figs. 5-7, it is obvious that with an increasing loading rate, the ultimate load carrying capacity of RC beams increases. The load carrying capacity of RC3_S0 increased by 20%, 52% and 66% respectively for low, medium and high rates of loading compared to the static load carrying capacity. The peak load was increased sharply in RC3_S0 and then fell instantly (brittle shear failure) for both static and low loading rates but the specimen had a significant amount of residual strength. However, the residual strength in the low loading rate was more than the static loading. Under medium and high rates, the load vs. mid-span deflection curve showed some indentation before reaching the peak load, indicating the development of cracking. One of the most important observations was the post-peak vibration of RC beam under medium and high loading rates. For RC3_S12 the peak load increased by 20%, 33% and 45% respectively for low, medium and high rates of loading in comparison to the static peak load. However, RC3_S12 (statically shear-critical) had enough amount of residual strength under static loading as compared to the other loading rate. For high rates, the residual strength was insignificant as compare to other rate of loading. It was observed that the slope of post-peak branch (i.e., descending branch) of the load-midspan deformation curve increased for high loading rates for shear-critical Specimens (RC3_S0 and RC3_S12). Similarly, for RC3_S56 load resistance increased by 7%, 11% and 15% respectively for low, medium and high rates of loading compared to the static case. A specific yield point was observed in RC3_S56 (statically flexure-critical) under static, low and medium loading rates whereas there was no yield point when the beam was subjected to a high loading rate. This could be due to some localized yielding of the reinforcing bar in the RC beam. Fig. 8(a) shows the variation of the peak load of each specimen under four different loading rates. Furthermore, the ultimate load carrying capacity of the RC beams increased with the increment of the shear reinforcement ratios. The dynamic increase factor (DIF) of RC beams under different loading rates is shown in Fig. 8(b). The average dynamic increase factor (i.e., the ratio of dynamic to static strength) was calculated to be 1.16, 1.36 and 1.42 for low, medium and high rates of loading respectively.

4.2.Stiffness

Considering the curves in Fig. 9(a), it appears that an increase in the loading rate led to an increase in the stiffness of the RC beams. This means that the specimens exhibited stiffer structural response due to the effect of increasing loading rates. RC3_S12 and RC3_S56 (with shear reinforcements) both exhibited stiffer structural response as compared to RC3_S0 (without shear reinforcements) under different loading rates. Therefore, it can be inferred that shear reinforcements had immense effect for stiffer structural response of RC beams, not only under static loading but also at loading rates higher than static loading. Based on the load vs. mid-span displacement curves of RC3_S0, it was observed that the specimen initially behaved elastically under medium and high loading rates and the first noticeable change in stiffness occurred at around 70

kN and 80 kN for medium and high loading rates respectively, indicating the development of cracking. For RC3_S12, the same phenomenon was observed at a high loading rate of around 90 kN (initiation of cracking) before it achieved its peak load. Deviation in stiffness (successive deterioration) was observed in RC3_S56 under high loading rates at around 95 kN and 150 kN due to some cracking before the specimen reached ultimate load carrying capacity. In general, under high rates of concentrated loading, RC beams exhibited very stiff structural response as compared to the static, low and medium loading rates.

4.3.Energy absorption

In calculating the area under the load vs. mid-span deflection curve (i.e., absorption energy), the generalized mid-span displacement range should be defined to impose the same conditions for all the specimens. For statically shear-critical beams RC3_S0 and RC3_S12, the deformation range was defined up to three times of the displacement corresponding to peak load-point displacement in the load vs. mid-span deflection curve. However, for statically flexure-critical beam RC3_S56, the deformation range was defined up to three times of the displacement corresponding to yield load-point displacement in the load vs. mid-span deflection curve for static, low and medium loading rates. But under high loading rate, the load vs. mid-span deflection curve of the specimens did not give any specific yield point. The influence of dynamic vibrations was observed in the experimentally obtained load vs. mid-span deflection relationships under high loading rate. For this reason, the displacement corresponding to the first peak point in the load vs. mid-span deflection relationships was used to calculate the area under this curve. The energy absorption capacity of the RC beams increased with the enhancement of loading rates. Moreover, transverse reinforcement had a significant effect in confining the core concrete; as a result, specimens having more transverse reinforcements (RC3_S56) absorbed more energy. Fig. 9(b) clearly illustrates the variation of the energy absorption capacity of RC beams for these four loading rates.

4.4.Strain at the mid-span of longitudinal tensile reinforcements and corresponding strain rates

After analyzing the strain history data of longitudinal tensile reinforcements and converting it to stress history by multiplying it by the elastic modulus of steel, it was recognized that the yield stress of tensile reinforcing bars was increased as compared to the static yield stress (371 MPa) for medium and high loading rates. For RC3_S0, 4% and 28% enhancement in yield stress in the tensile reinforcing bars was observed in the case of medium and high loading rates respectively. Similarly, it was calculated to be 7% and 25% more than the static yield stress of the tensile reinforcing bars of RC3_S12 for medium and high loading rates respectively. Again for RC3_S56, 40%, 49% and 54% increment in yield stress in the tensile reinforcing bars were observed for low, medium and high loading rates respectively. The strain rate at the early stage of loading was very high, then it reduced abruptly only under high loading rate. Extreme localized yielding of reinforcing bars due to enhanced bond properties at high loading rate could be the reason for that. The peak strain rates (at the mid-span of longitudinal tensile reinforcements) were computed to be 0.0052/s, 0.084/s, 0.57/s and 5.1/s for static, low, medium and high

rates of loading respectively for RC3_S0. Similarly, the peak strain rates were calculated to be 0.0049/s, 0.084/s, 0.4/s and 3.1/s for static, low, medium and high rates of loading respectively for RC3_S12. Again for RC3_S56, peak strain rates were computed to be 0.0023/s, 0.088/s, 0.3/s and 6.1/s for static, low, medium and high rates of loading respectively. Approximately, an increment by one order (10 times) in the peak strain rate was observed as the loading rates progressed from low to high. Kulkarni and Shah tested RC beams for high rate at a piston velocity of 0.38 m/s. It is analogous to the medium rates (0.40 m/s) of loading to RC beams in the present study. The average strain rate was computed to be 0.3/s under high loading rate by Kulkarni and Shah, which is also in close agreement with our medium rate of loading where an average strain rate of approximately 0.1/s was observed in the mid-span of the tensile longitudinal reinforcement. To correlate the peak strain rate $(\dot{\varepsilon})$ and loading rate (δ), a simplified equation can be proposed by analyzing the experimental data,

$$\dot{\varepsilon} = 1.25 * \delta^{0.82} \quad (1)$$

This equation could be very useful in analytical analysis and/or finite element simulation of RC beams to calculate the DIF of yield and ultimate stress of tensile reinforcements under varying loading rates.

4.5.Crack patterns

The high-resolution digital photography and high-speed camera produced images of the side surface of RC beams that yielded detailed deflection and a visual record of the crack patterns under four different loading rates. RC3_S0 exhibited compression strut failure under static loading. For low rates of loading, the same type of failure followed by spalling of concrete occurred at the bottom of the specimens. The longitudinal bars were exposed and bent. There were also signs of bond failure of the reinforcement bars at the supports. After bending, the longitudinal bar almost disintegrated the cover concrete. In the case of medium rates of loading, the beam divided in two parts and the exposed longitudinal bars were bent. Severe damage occurred for high rates of loading. Concrete cover below the tensile reinforcement region around the support at one side spalled off. RC3_S12 exhibited diagonal cracks on both sides from the loading point to the support but one side was much wider than the other under static loading. The beams were disintegrated into two components along the diagonal cracks and the longitudinal bars were severely bent under low loading rate. Almost the same failure mode was visualized for medium loading rate. Massive damage occurred for high rates of loading. Diagonal shear cracks were observed in both sides but they were not symmetric in terms of their crack width. One side was totally damaged with exposed longitudinal bars, spalling of concrete cover and bond failure at the support. After critical observation of failure modes of two shear-critical beams (RC3_S0 and RC3_S12), it is determined that more catastrophic failure (i.e. disintegration of beam, spalling of concrete and exposure of reinforcing bars) was perceived as the loading rates proceeded from static to high. The crushing and spalling of compression concrete was examined for RC3_S56 under static load. Also few diagonal cracks and several flexural cracks were observed. For low rates of loading, flexural and few diagonal cracks were noticed. The rate of progress of flexural cracks was reduced with the crushing of the concrete in the top compression fibers. Several flexural cracks were visualized and compression concrete was crushed under

medium rates of loading. Same type of failure mode was also observed for high rates of loading. The failure mode of RC3_S56 (statically flexure-critical) was not so catastrophic for loading rates higher than static loading in contrast to shear-critical beams. Another interesting observation was that under medium and high loading rates, the damaged portion of RC3_S56 mostly affected by the application of the external load tended to be concentrated in the region of the load-point at the mid-span; in contrast for the static and low loading rates, the crack distribution seemed to extend nearly to the supports. That means that as the loading rate increased, the portion of the beam in which the cracks occurred became narrower.

5. FEM analysis of RC beams under different rates of concentrated loading

LS-DYNA was employed in this study because of its proven effectiveness in geometric modeling and analysis capability under high rates of concentrated loading. The adoption of 3D analysis arose from the need to account sufficiently for the effects of inertia and the nonlinear behavior of concrete and steel. The description of modeling includes structural geometry, boundary conditions, application of loads, and relevant material models.

5.1.Structural geometry

Fig. 10 shows the three-dimensional FE model of tested RC beams. Eight node solid hexahedron elements with a single integration point were used to represent concrete while beam elements (2-node Hughes-Liu beam element formulation with 2 x 2 Gauss quadrature integration) were used to model steel reinforcing bars. Comparing the pre-analysis results with the experimental ones, the mesh geometry was chosen as follows considering the fact that the mesh aspect ratio is smaller than 1.5. A mesh size of 25 mm was used to create the solid element in the span direction of RC beam whereas the mesh configuration in sectional directional comprised: (1) in the depth direction of RC beam, 8 elements for concrete between the top and bottom longitudinal reinforcements and 2 elements for concrete cover; (2) in the width direction, 4 elements between two adjoining longitudinal reinforcements and 2 elements for concrete cover. In total, approximately, 9300 nodal points and 7300 elements were used to model the whole structures. The mesh discretization was so established that the reinforcement nodes coincided with the concrete nodes. The steel reinforcing bars were modeled explicitly using beam elements connected to the concrete mesh nodes. The nodes that linked the concrete and reinforcement mesh were shared and therefore unable to slip. Due to this assumption of complete compatibility of strains between the concrete and steel nodes, they formed a perfect bond.

5.2.Boundary conditions and application of load

To simulate the actual experimental conditions, the beams were supported on two rigid cylinders made of solid elements. Constraints were defined to the support cylinder, so that it could rotate about its own longitudinal axis but would not be able to translate. Displacement was prescribed in the rigid loading plates located at the mid-span of the RC beam. The rigid loading plate was allowed to move only in the vertical direction. The prescribed displacement was linear, going from zero displacement to 40 mm

displacement under certain time duration, depending on the desired rate of loading. The corresponding applied load due to the prescribed displacement was then determined by monitoring the vertical reaction forces at the concrete nodes in contact with the support solid cylinders. The algorithm CONTACT_AUTOMATIC_SINGLE_SURFACE in LS-DYNA was used to model the contact between the support cylinder, loading plate and RC beam. This algorithm automatically generates slave and master surfaces and uses a penalty method where nominal interface springs are used to interpenetration between element and surfaces. The interface stiffness is computed as a function of the bulk modulus, volume and face area of the elements on the contact surface.

5.3.Modeling of materials

5.3.1. Concrete

Material type 072 R3 (MAT_CONCRETE_DAMAGE_REL3), was the third release of Karagozian and Case (K&C) concrete model was utilized in this study. It includes the implementation of a third, independent yield failure surface, removal of tension cutoff and extension of the plasticity model in tension; shift of the pressure cutoff; implementation of the three invariant formulation for the failure surfaces; determination of the triaxial extension to triaxial compression ratio as a function of pressure; shear modulus correction and implementation of a radial path strain rate enhancement [12]. A comprehensive material model of concrete was provided by Wu et al. [13]. The model can generate default parameters based on the negative value of unconfined compressive strength of the concrete, density of concrete and unit conversion factor for length and stress. Details of this default model parameter generation feature were provided by Schwer & Malver [14].

5.3.2. Steel reinforcement

The steel reinforcement bars (longitudinal and shear reinforcements) within the beam were modeled as a strain sensitive uniaxial elastic-plastic material to account for its strain rate sensitivity as well as stress-strain history dependence. Material model PIECEWISE_LINEAR_PLASTICITY (MAT_024) from LS-DYNA was employed in this study to incorporate the strain rate effect. Wu et al. vividly depicted the details of the steel material modeling. The expressions proposed by Malvar [15] on strain rate effect were utilized in this study.

5.3.3. Loading plate, support roller and plate

MAT_RIGID (MAT_020) was used from LS-DYNA material library to model the loading plates, support rollers and plates. Realistic values of Young's modulus and Poisson's ratio of the rigid material should be defined since unrealistic values may contribute to numerical problems in contact. Young's modulus and Poisson's ratio of steel material were used for the rigid material in the numerical simulation.

6. Verification of finite element analysis results

Numerical simulation results of reinforced concrete beams subjected to four different loading rates were calibrated with the experimental results of the present study. Moreover,

one pair of RC beams (B4JL25-S and B4JL25-H) was taken from Kulkarni & Shah for further validation of the FE results under static and high loading rates.

6.1.Load vs. mid-span deflection of reinforced concrete beams

To simulate experimental conditions, the beams were analyzed in displacement control in LS-DYNA. Figs. 11-13 present the comparisons of the numerical simulations results with experiments of the load vs. mid-span deflection of RC beams under four different rates of loading conditions. Fig. 14 depicts the comparisons of the load vs. mid-span displacement of Specimen B4JL25 obtained from the published experimental results by Kulkarni & Shah under static (0.0000071 m/s) and high rates (0.38 m/s) of loading. The comparisons were considered to be in reasonably good agreement except for the Specimen RC3_S56 under high loading rates.

6.2.Crack profiles on side surface of RC beams

The damage of the RC beams by numerical simulation is shown by plotting the fringes of effective plastic strain. These effective plastic strain contours reveal the strain localization where failure propagates. Fig. 15 shows the cracking pattern of the RC beams of the present study compared with the damage plot of numerical simulation results. The comparative damage plot of RC beams tested by Kulkarni & Shah is also shown in Fig. 16. From these comparisons, it can be enunciated that the damage plot of numerical simulation results can capture the experimental crack profiles of RC beams under varying loading quite satisfactorily.

7. Numerical simulation parametric study

7.1.Numerical simulation matrix

After verification of the FE model against the experimental results, this section presents a parametric investigation to elucidate more information about the behavior of RC beams under varying loading rates. The response of the RC beams was studied by varying some key parameters such as shear span to effective depth ratios (a/d: 3.3 and 4.4), longitudinal reinforcement ratios (ρ_g: 2.4% and 1.27%), transverse reinforcement ratios (ρ_v: 0%, 0.12%, 0.20% and 0.56%) and loading rates (δ: 0.0004, 0.04, 0.4 and 2 m/s). Fig. 17 illustrates the general schematic diagram of the RC beams and Table 2 summarizes the specimen characteristics of the simulation matrix.

7.2.Influence of longitudinal reinforcement ratio

Fig. 18 illustrates the effect of the longitudinal reinforcement ratio on the DIF of maximum resistance of RC beams under varying loading rates. Specimens without transverse reinforcements did not exhibit any influence on the DIF of the RC beams for different longitudinal reinforcement ratios, whereas specimens having transverse reinforcements showed some differences in the DIF of RC beams under varying loading rates. There were two types of RC beams in terms of their slenderness ratio (a/d - 3.3 & 4.4). Fig. 18 shows that the DIF was observed to be on the higher side with low

longitudinal reinforcement ratio (1.27%) of the RC beams for low, medium and high loading rates. This may be in contrary to the fact that as the longitudinal reinforcement ratio increases, both the ultimate moment capacity as well as the ultimate load carrying capacity increase. It is true that for specimens having low longitudinal reinforcement ratio (1.27%), the ultimate load carrying capacity is always lower than specimens having high longitudinal reinforcement ratio (2.4%). But the DIF increased with decreasing longitudinal reinforcement ratio of RC beam as the loading rate progressed from static to high. This means that although the peak load is less in the RC beam with low longitudinal reinforcement ratio for all loading rates, but the rate of increment of ultimate load carrying capacity was higher as compared to high longitudinal reinforcement contained in the RC beams. With a low reinforcement ratio in the RC beam, there is a corresponding increase in the loading rate sensitivity, potentially causing an enhancement of the DIF.

7.3.Influence of transverse reinforcement ratio

The DIF of RC beams without transverse reinforcements increased linearly whereas for the case of transverse reinforcements, it increased exponentially as shown in Fig. 19. A significant increase in DIF was observed in the high loading rate (2 m/s) for RC beams having high amount (0.56%) of transverse reinforcements. In general, it seemed that transverse reinforcements have insignificant effects on the DIF of RC beams (shear span to effective depth ratio - 4.4) under low and medium loading rates. Nevertheless, high amount of transverse reinforcement ratio (0.56%) in RC3_S56 beam resisted the catastrophic failure mode (i.e., huge cracking and spalling of concrete, and exposure and bending of longitudinal reinforcements) under loading rates greater than static loading, by providing additional confinement to the core concrete and supplementing lateral restraint capacity against buckling of the longitudinal reinforcements.

7.4.Influence of shear span to effective depth ratio

In this study, the cross-section was kept constant for all the beam specimens. An increase in beam shear span to effective depth ratio meant an increase in span length. As a result, maximum load carrying capacity will increase with increasing shear span to effective depth ratio for the same amount of the longitudinal reinforcement ratio. The effect of shear span to effective depth ratio on the DIF of the RC beam is shown in Fig. 20. It is perceived that for the same amount of longitudinal reinforcements in a RC beam, the DIF would increase with the enhancement of the shear span to effective depth ratio.

7.5.Proposed equations for evaluation of DIF of maximum resistance of RC beam under varying loading rates

A parametric study revealed the significance of parameters that affect the DIF of maximum resistance of RC beams under varying loading rates. Two empirical equations were proposed through multivariable regression analysis in terms of various parameters to predict the DIF. The empirical equation for RC beams without transverse reinforcements is expressed as follows:

$$\mathrm{DIF} = \left[0.004\rho_g + 0.136(a/d) - 0.34\right]\log_e\delta + \left[0.009\rho_g + 0.41(a/d) + 0.157\right] \quad (2)$$

The other empirical equation for the case of RC beams having transverse reinforcements is depicted as follows:

$$\mathrm{DIF} = \left[1.89 - 0.067\rho_g - 0.42\rho_v - 0.14(a/d)\right] e^{\left[-0.35-0.052\rho_g+0.179\rho_v+0.18(a/d)\right]\delta} \quad (3)$$

Examples presenting the comparison of proposed equations with the numerical analysis results are presented in Fig. 21. The solid and dotted lines in each plot denote the proposed equations, while the scatter data points represent the numerical analysis results. After inspecting the plots, it can be addressed that for most of the cases, the proposed equations are in close agreement with the numerical analysis results.

8. Conclusions

Based on the results presented in this paper, the following conclusions were drawn:

- The ultimate load carrying capacity, stiffness and energy absorption of RC beams were found to increase along with the loading rates. The ultimate load carrying capacity of the RC beams also increased with the increment of shear reinforcement ratios. It was observed that the slope of the post-peak branch (i.e., descending branch) of the load-midspan deformation curve increased for high loading rates for shear-critical RC beams (RC3_S0 and RC3_S12).
- A simplified equation was proposed to correlate the peak strain rate and loading rate which could be very useful in calculating the DIF of yield and ultimate stress of tensile reinforcements in RC beam under varying loading rates. Peak strain rate was amplified in one order of magnitude (approximately, 10 times) as the loading rates progressed from low to high. The strain rate at the early stage of loading was very high, then it reduced abruptly only in the case of high loading rate.
- Shear-critical RC beams (RC3_S0 & RC3_S12) exhibited more catastrophic failure modes for loading rates higher than static loading, including the fragmentation of beams into several pieces, exposure and bending of longitudinal reinforcements and massive cracking and spalling of concrete. In contrast, flexure-critical beams (RC3_S56) had a much milder response (failure mode) under loading rates higher than static loading.
- The DIF increased with decreasing longitudinal reinforcement ratio of RC beam as the loading rate progressed from static to high. With a low reinforcement ratio in the RC beam, there is a corresponding increase in the loading rate sensitivity, potentially causing an enhancement of the DIF. With the same amount of longitudinal reinforcements in a RC beam, DIF increased with the enhancement of shear span to effective depth ratio.
- A significant influence of the transverse reinforcement ratio on DIF was observed for the RC beam under high loading (2 m/s) rate. High amount of transverse reinforcement ratio (0.56%) in the RC3_S56 beam resisted the catastrophic failure mode under loading rate greater than static loading by providing additional confinement to the core concrete and supplementing lateral restraint capacity against the buckling of the longitudinal reinforcements.
- Two empirical equations were proposed in terms of various parameters by multivariable regression analysis to predict the DIF of maximum resistance of RC under varying loading rates. Comparison of the proposed equations with the numerical analysis results demonstrated that the proposed curves delineated the inclination of the DIF of RC beams

under varying loading rates quite accurately. However, more refinement is needed in FE model to accurately plot the post-peak branch of load vs. mid-span deflection curve. Moreover, future experimental investigation of RC beams under varying loading rates is indeed necessary and should consider other parameters such as varying grades of concrete and steel reinforcing bars for further incorporation of these parameters in the proposed equations.

References

[1] Bing LR, Park R, Tanaka H. Constitutive behavior of high strength concrete under dynamic loading. ACI Structural Journal July-August 2000; 97: 619-29.

[2] Bhatti AQ, Kishi N. Impact response of RC rock-shed girder with sand cushion under falling load. Journal of Nuclear Engineering and Design October 2010; 240:2626-32.

[3] Bhatti AQ, Kishi N, Mikami H, Ando T. Elasto-plastic impact response analysis of shear-failure type RC beams with shear rebars. Journal of Materials & Design 2009; 30: 502-10.

[4] Kishi N, Bhatti AQ. An equivalent fracture energy concept for nonlinear dynamic response analysis of prototype RC girders subjected to falling-weight impact loading. International Journal of Impact Engineering January 2010; 37(1):103-13.

[5] Bhatti AQ, Kishi N, Mikami H. An applicability of dynamic response analysis of shear-failure type RC beams with lightweight aggregate concrete under falling-weight impact loading. Journal of Materials and Structures Jan 2011; 44(1):221-31. Springer.

[6] Saatci S, Vecchio F. Nonlinear finite element modeling of reinforced concrete structures under impact loads. ACI Structural Journal 2009; 106(5):717-25.

[7] Kulkarni SM, Shah SP. Response of reinforced concrete beams at high strain rates. ACI Structural Journal 1998;95(6):705-15.

[8] Fujikake K, Li B, Soeun S. Impact response of reinforced concrete beam and its analytical evaluation. ASCE Journal of Structural Engineering August 2009; 135(8):938-50.

[9] LS-DYNA. Keyword user's manual, version 971. U.S.A.: LST Corp.; 2007.

[10] Mutsuyoshi H, Machida A. Properties and failure of reinforced concrete members subjected to dynamic loading. Transactions of the Japan Concrete Institute 1984; 6: 521-8.

[11] ACI Committee 318. Building code requirements for structural concrete (ACI 318-08) and commentary. Farmington Hills, Mich: American Concrete Institute; 2008.

[12] Malvar LJ, Crawford JE, Wesevich JW, Simons D. A plasticity concrete material model for DYNA3D. International Journal of Impact Engineering June 1997;19: 847-73.

[13] Wu Ke-Chiang, Li B, Tsai Keh-Chyuan. Residual axial compression capacity of localized blast-damaged RC columns. International Journal of Impact Engineering Jan 2011; 38: 29-40.

[14] Schwer LE, Malver LJ. Simplified concrete modeling with *Mat_Concrete_Damage_Rel3. JRI LS-DYNA User Week; August 2005.

[15] Malvar LJ. Review of static and dynamic properties of steel reinforcing bars. ACI Materials Journal 1998; 95 (5):609-16

List of Tables

List of Figures

Serial No.	Designation	Shear span to effective depth ratio	Longitudinal rebar ratio (%)	Shear rebar ratio (%)	Flexural resistance (kN)	Shear resistance (kN)	Shear to bending resistance ratio	Expected failure mode
1	RC3_S0	3.33	2.41	0	148.65	65.39	0.44	Shear
2	RC3_S12	3.33	2.41	0.12	148.65	88.44	0.59	Shear
3	RC3_S56	3.33	2.41	0.56	148.65	181.2	1.22	Flexure

Table 1

Table 2

Beam mark	Beam specifications						Shear span to effective depth ratio		Longitudinal reinforcement						Shear reinforcement			Shear to bending resistance ratio
	f_c' (MPa)	h (mm)	b (mm)	d (mm)	a (mm)	L (mm)	a/d	L/h	Top			Bottom			Diameter (mm)	Ratio (%)	f_y (Mpa)	
									Diameter (mm)	Ratio (%)	f_y (Mpa)	Diameter (mm)	Ratio (%)	f_y (Mpa)				
[a]RC3_SO_1	40	250	150	210	700	1700	3.3	6.8	2T22	2.4	371	2T22	2.4	371	R6	0	342	0.45
[a]RC3_S12_1									2T22	2.4		2T22	2.4			0.12		0.60
RC3_S20_1									2T22	2.4		2T22	2.4			0.20		0.75
[a]RC3_S56_1									2T22	2.4		2T22	2.4			0.56		1.22
RC3_SO_2									2T16	1.27		2T16	1.27			0		0.79
RC3_S12_2									2T16	1.27		2T16	1.27			0.12		1.07
RC3_S20_2									2T16	1.27		2T16	1.27			0.20		1.33
RC3_S56_2									2T16	1.27		2T16	1.27			0.56		2.18
RC4_SO_1	40	250	150	210	900	2100	4.4	8.4	2T22	2.4	371	2T22	2.4	371	R6	0	342	0.57
RC4_S12_1									2T22	2.4		2T22	2.4			0.12		0.77
RC4_S20_1									2T22	2.4		2T22	2.4			0.20		0.96
RC4_S56_1									2T22	2.4		2T22	2.4			0.56		1.57
RC4_SO_2									2T16	1.27		2T16	1.27			0		1.02
RC4_S12_2									2T16	1.27		2T16	1.27			0.12		1.38
RC4_S20_2									2T16	1.27		2T16	1.27			0.20		1.71
RC4_S56_2									2T16	1.27		2T16	1.27			0.56		2.80

Note: T — Deformed bar, R — Plain bar; f_y — Yield strength of reinforcements; f_c' — Compressive strength of concrete.

[a] Experimental specimens.

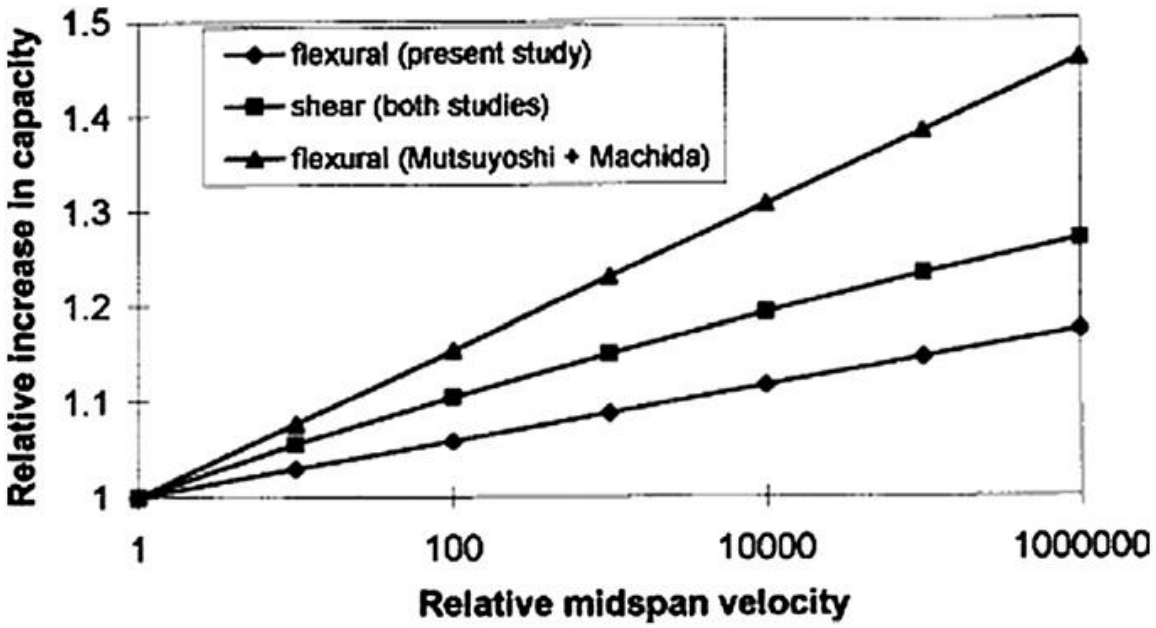
Relative increase in capacity
1.5
1.4
1.3
1.2
1.1
1
flexural (present study)
shear (both studies)
flexural (Mutsuyoshi + Machida)
1
100
10000
1000000
Relative midspan velocity

Fig. 1

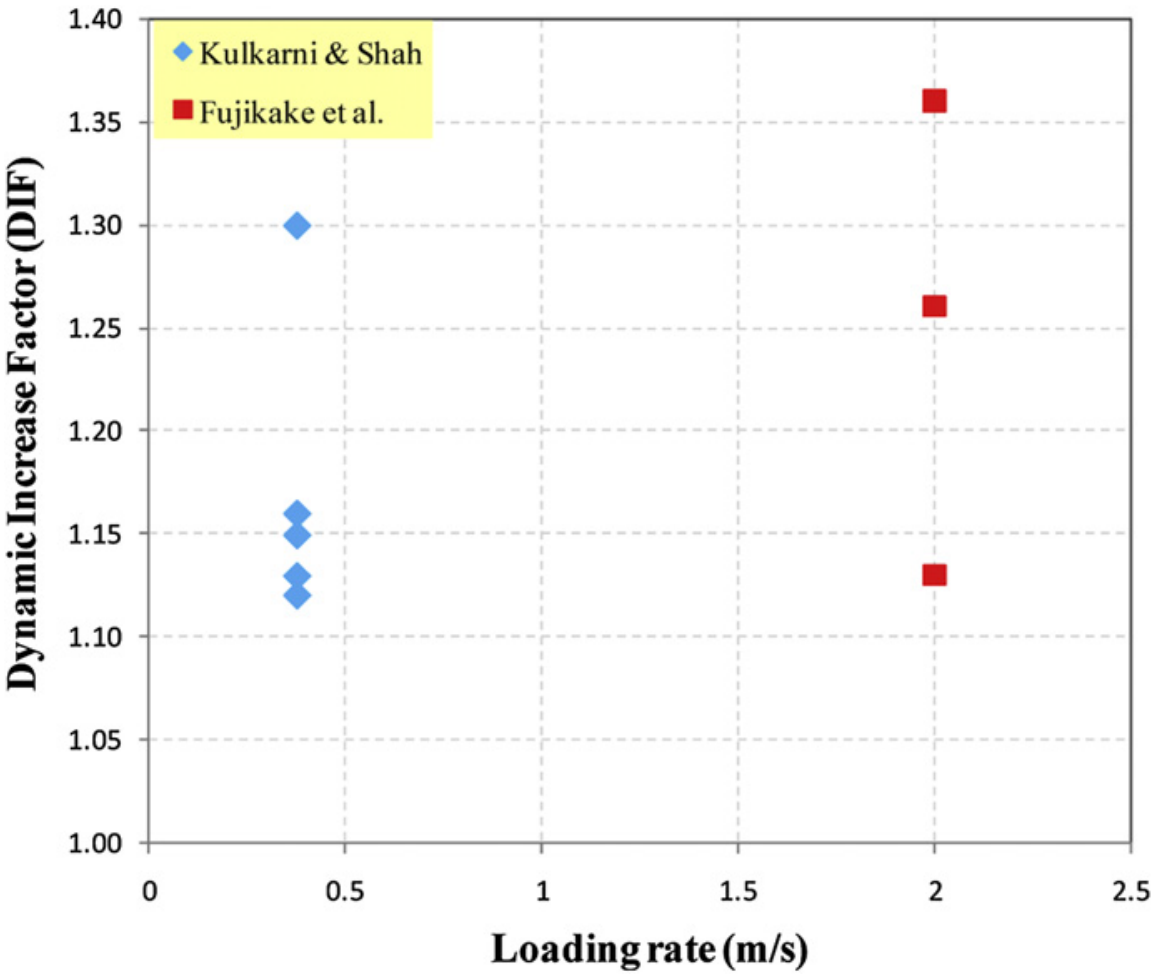
Kulkarni & Shah
Fujikake et al.
Dynamic Increase Factor (DIF)
1.40
1.35
1.30
1.25
1.20
1.15
1.10
1.05
1.00
0
0.5
1
1.5
2
2.5
Loading rate (m/s)

Fig. 2

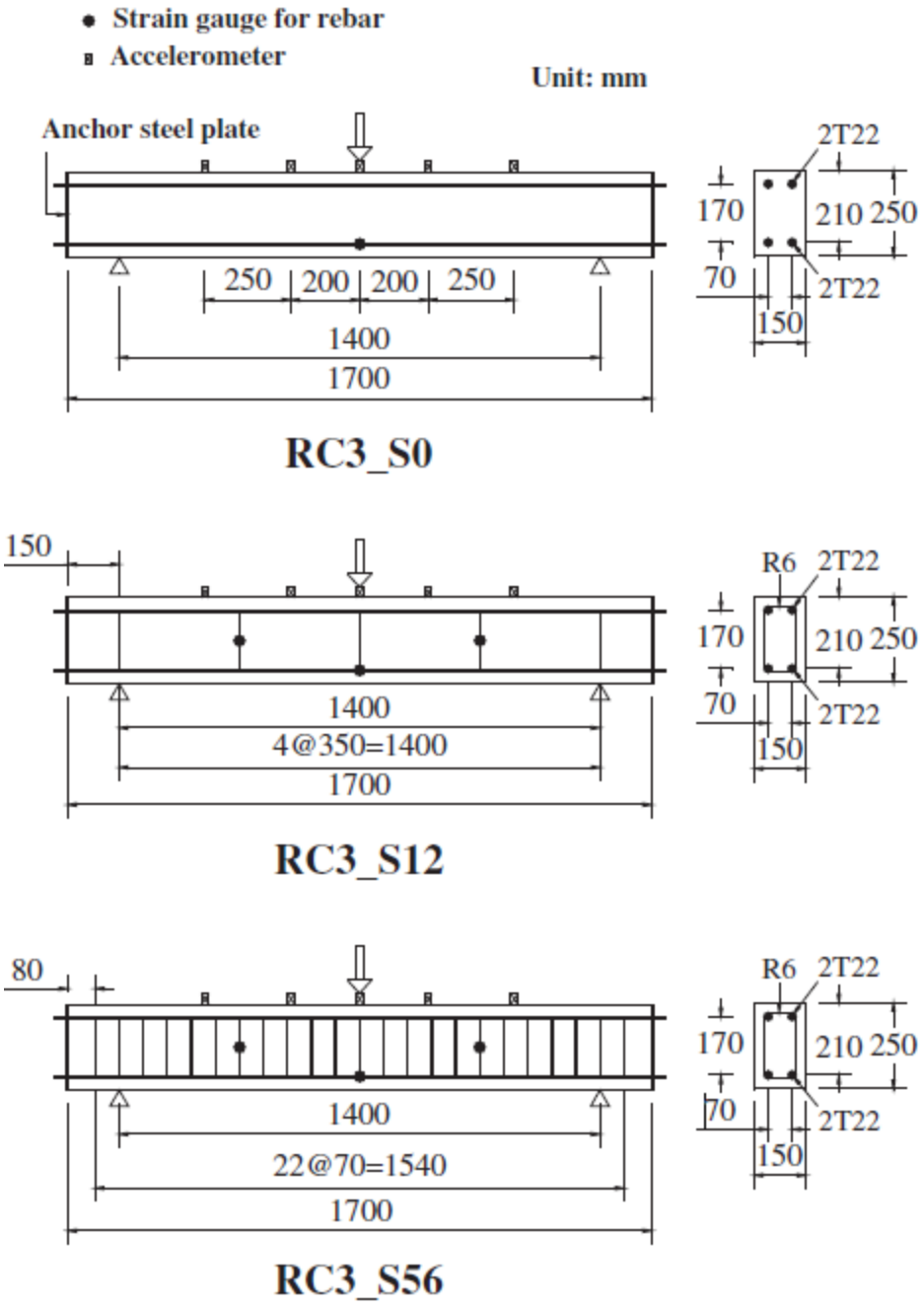
Strain gauge for rebar
Accelerometer
Unit: mm
Anchor steel plate
250
200
200
250
1400
1700
2T22
170
210 250
70
2T22
150
RC3_S0
150
1400
4@350=1400
1700
R6
2T22
170
210 250
70
2T22
150
RC3_S12
80
1400
22@70=1540
1700
R6
2T22
170
210 250
70
2T22
150
RC3_S56

Fig. 3

Fig. 4

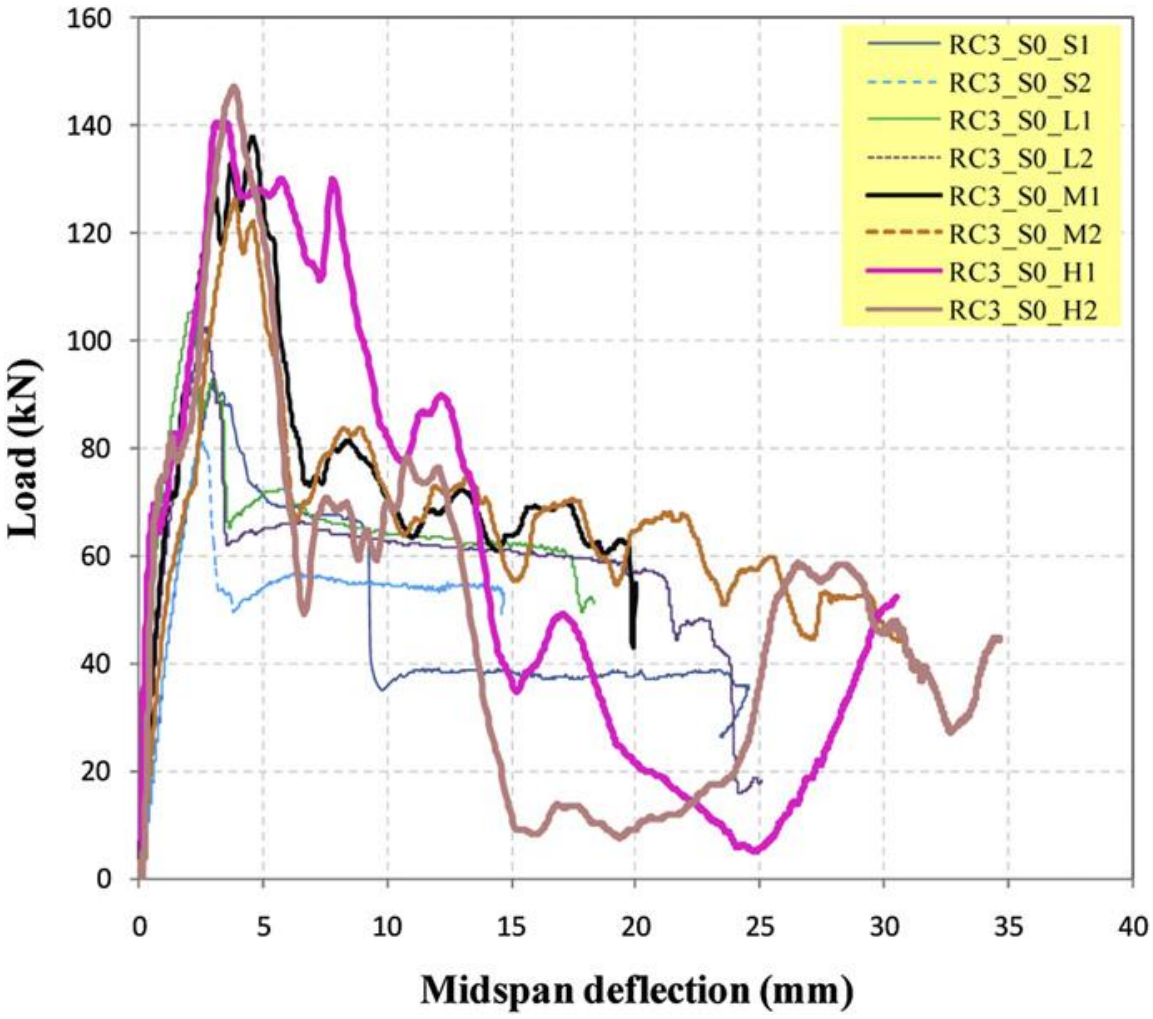
RC3_S0_S1
RC3_S0_S2
RC3_S0_L1
RC3_S0_L2
RC3_S0_M1
RC3_S0_M2
RC3_S0_H1
RC3_S0_H2
Load (kN)
Midspan deflection (mm)
0
20
40
60
80
100
120
140
160
0
5
10
15
20
25
30
35
40

Fig. 5

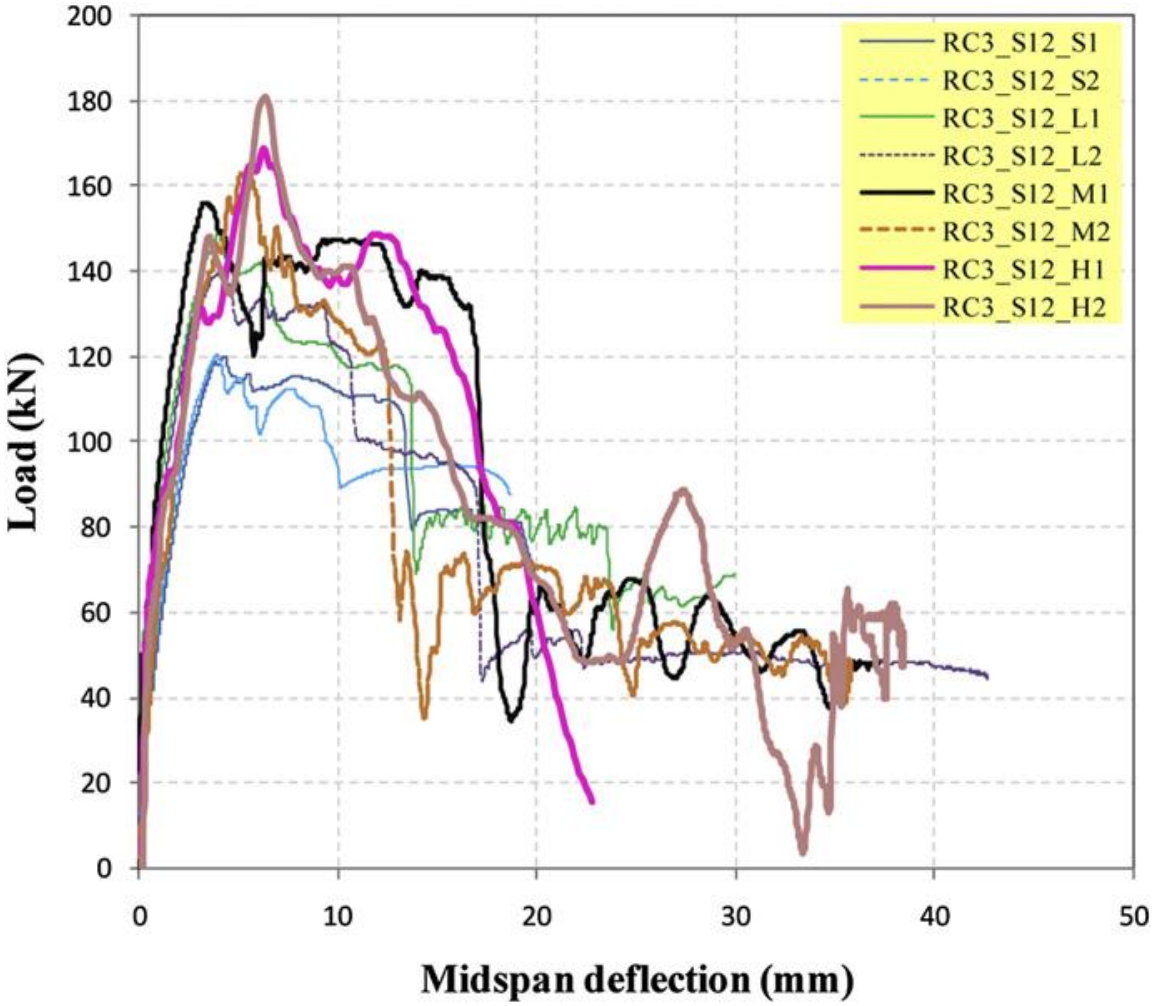
RC3_S12_S1
RC3_S12_S2
RC3_S12_L1
RC3_S12_L2
RC3_S12_M1
RC3_S12_M2
RC3_S12_H1
RC3_S12_H2
Load (kN)
Midspan deflection (mm)
0
20
40
60
80
100
120
140
160
180
200
0
10
20
30
40
50

Fig. 6

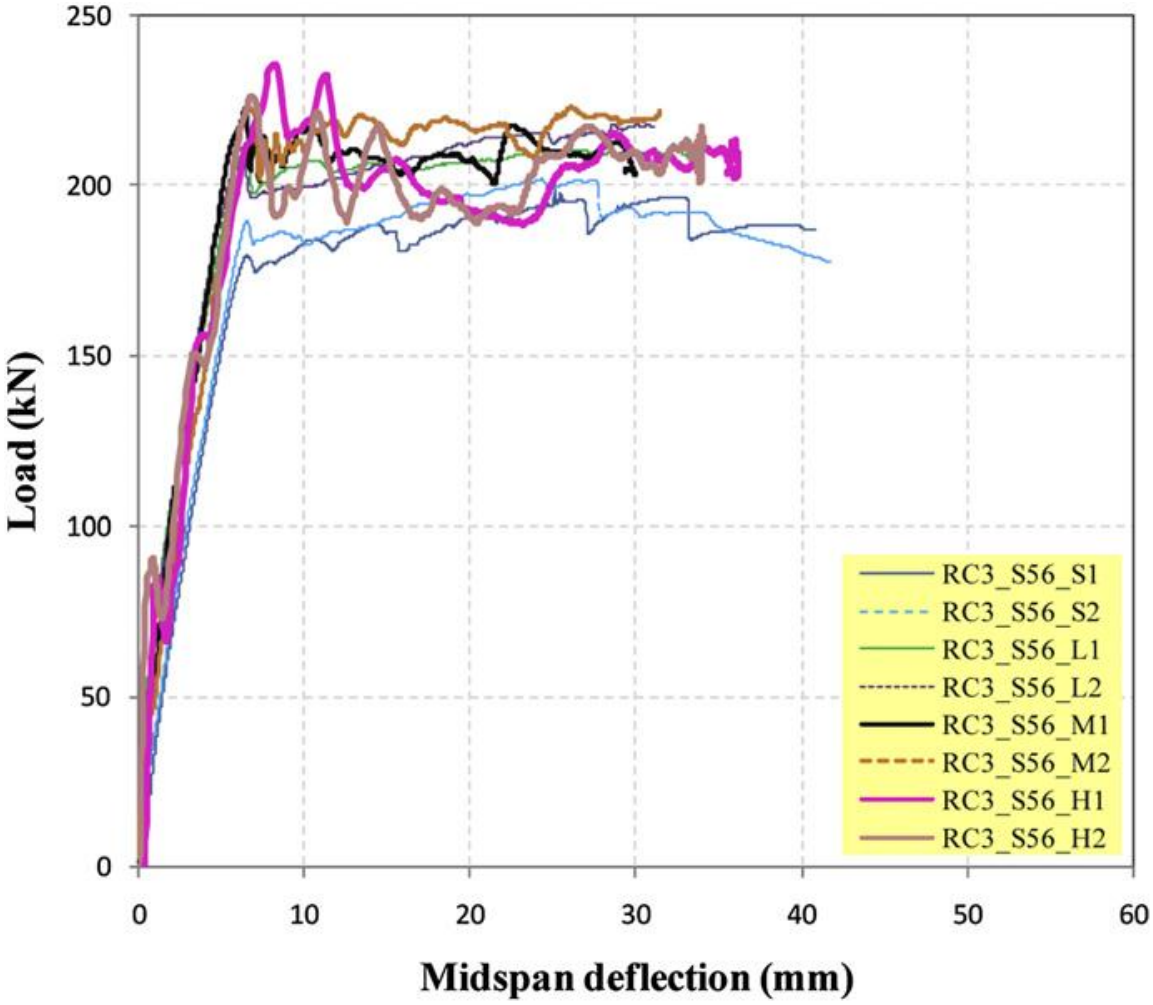
250
200
150
100
50
0
Load (kN)
0
10
20
30
40
50
60
Midspan deflection (mm)
RC3_S56_S1
RC3_S56_S2
RC3_S56_L1
RC3_S56_L2
RC3_S56_M1
RC3_S56_M2
RC3_S56_H1
RC3_S56_H2

Fig. 7

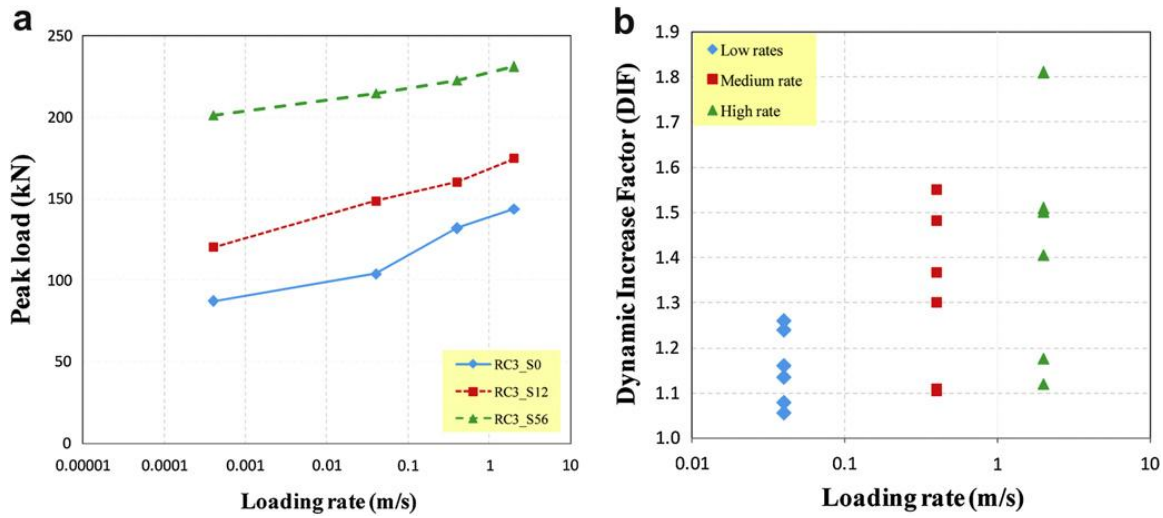
a
Peak load (kN)
250
200
150
100
50
0
0.00001
0.0001
0.001
0.01
0.1
1
10
Loading rate (m/s)
RC3_S0
RC3_S12
RC3_S56
b
Dynamic Increase Factor (DIF)
1.9
1.8
1.7
1.6
1.5
1.4
1.3
1.2
1.1
1.0
0.01
0.1
1
10
Loading rate (m/s)
Low rates
Medium rate
High rate

Fig. 8

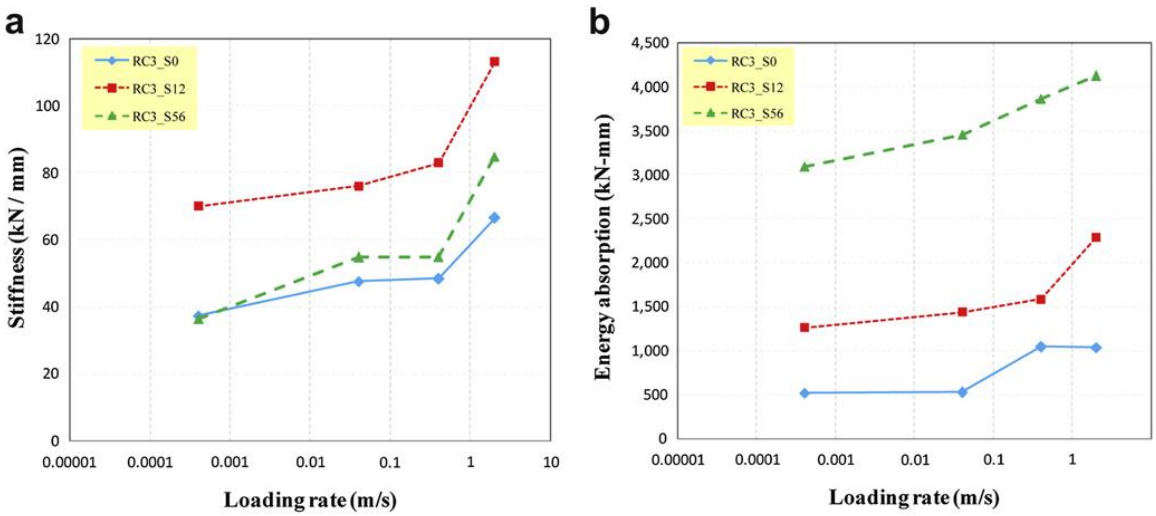
a
Stiffness (kN / mm)
120
100
80
60
40
20
0
RC3_S0
RC3_S12
RC3_S56
0.00001
0.0001
0.001
0.01
0.1
1
10
Loading rate (m/s)
b
Energy absorption (kN-mm)
4,500
4,000
3,500
3,000
2,500
2,000
1,500
1,000
500
0
RC3_S0
RC3_S12
RC3_S56
0.00001
0.0001
0.001
0.01
0.1
1
Loading rate (m/s)

Fig. 9

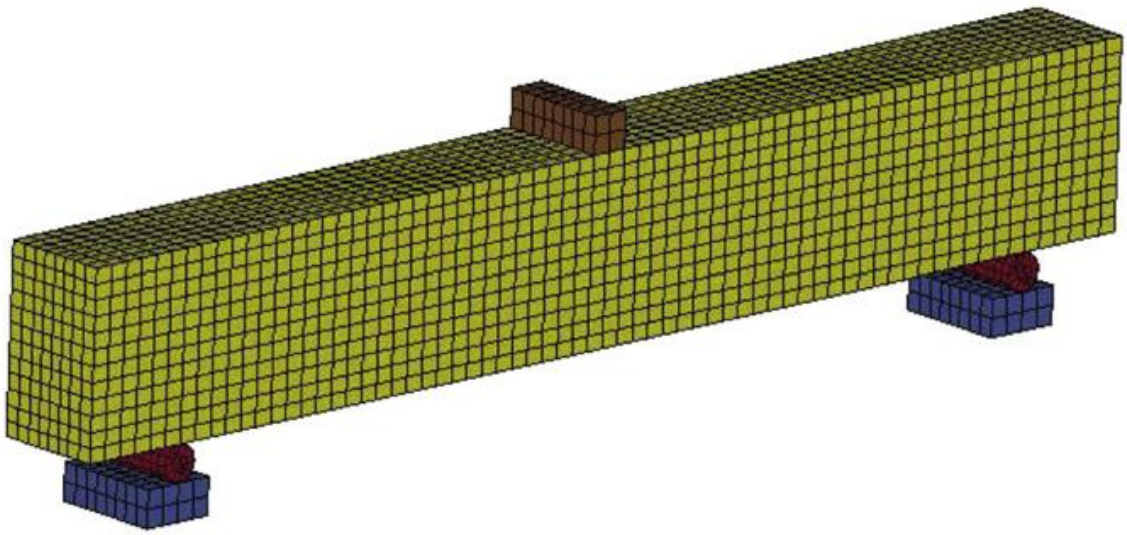

Fig. 10

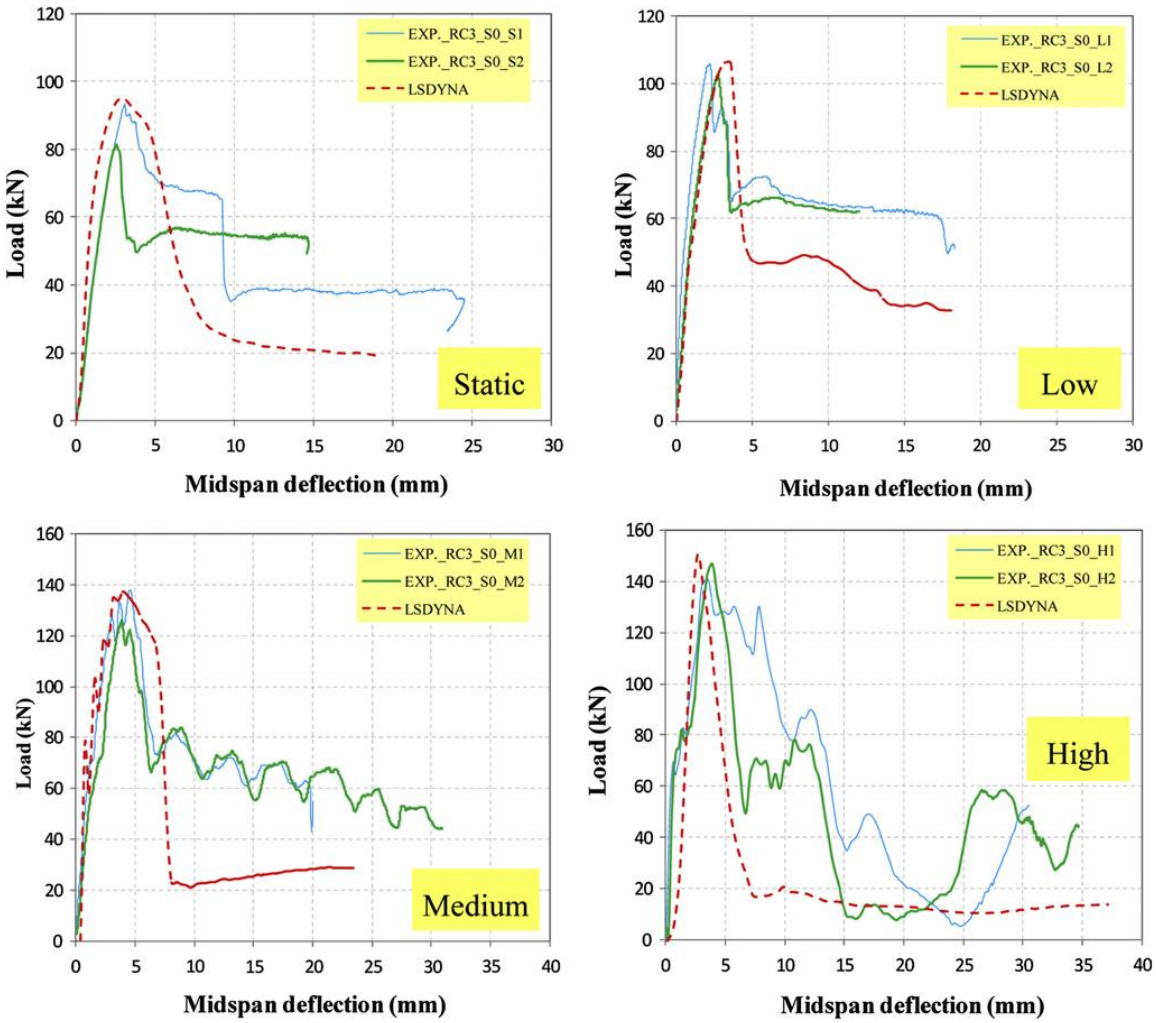
EXP._RC3_S0_S1
EXP._RC3_S0_S2
LSDYNA
Static
Load (kN)
Midspan deflection (mm)
EXP._RC3_S0_L1
EXP._RC3_S0_L2
LSDYNA
Low
Load (kN)
Midspan deflection (mm)
EXP._RC3_S0_M1
EXP._RC3_S0_M2
LSDYNA
Medium
Load (kN)
Midspan deflection (mm)
EXP._RC3_S0_H1
EXP._RC3_S0_H2
LSDYNA
High
Load (kN)
Midspan deflection (mm)

Fig. 11

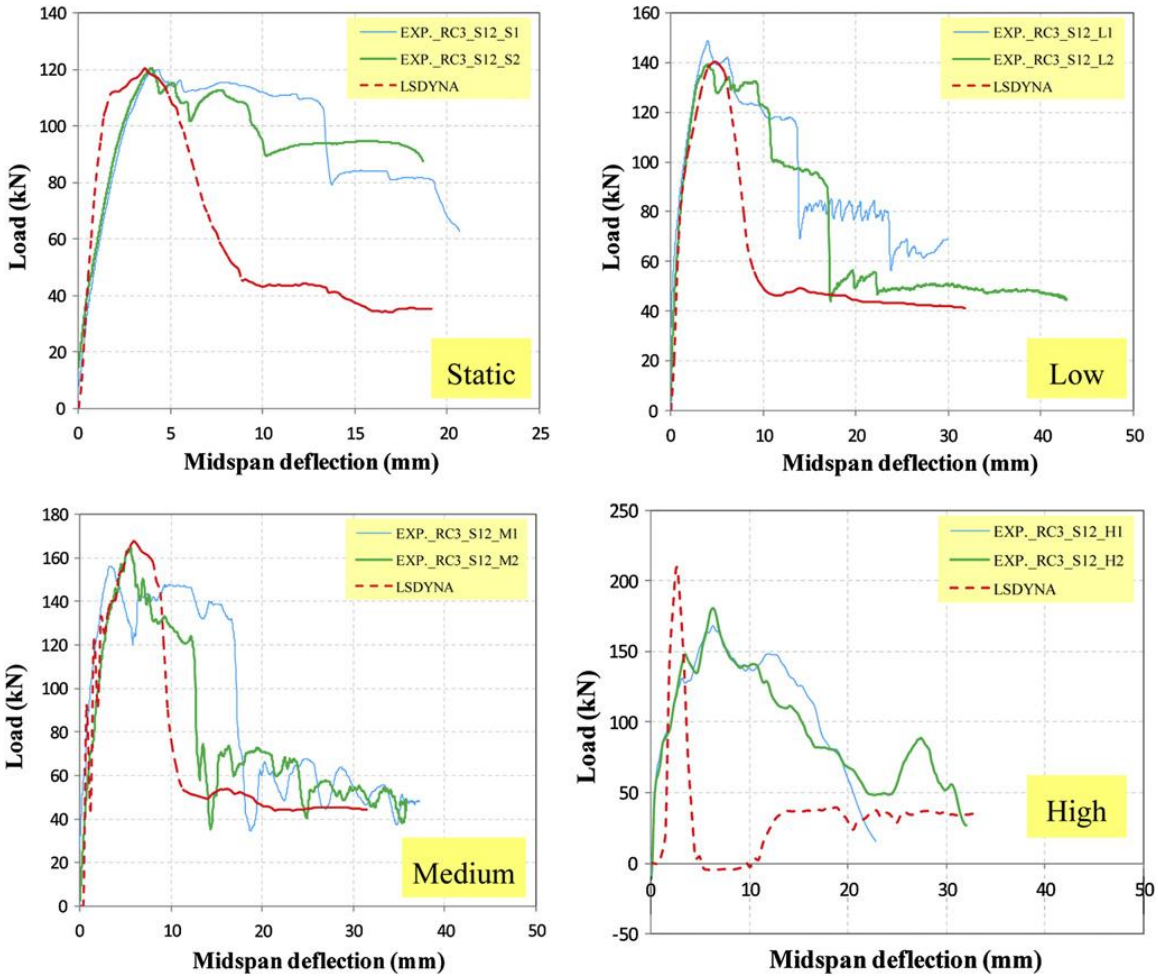
EXP._RC3_S12_S1
EXP._RC3_S12_S2
LSDYNA
Static
Load (kN)
Midspan deflection (mm)
EXP._RC3_S12_L1
EXP._RC3_S12_L2
LSDYNA
Low
Load (kN)
Midspan deflection (mm)
EXP._RC3_S12_M1
EXP._RC3_S12_M2
LSDYNA
Medium
Load (kN)
Midspan deflection (mm)
EXP._RC3_S12_H1
EXP._RC3_S12_H2
LSDYNA
High
Load (kN)
Midspan deflection (mm)

Fig. 12

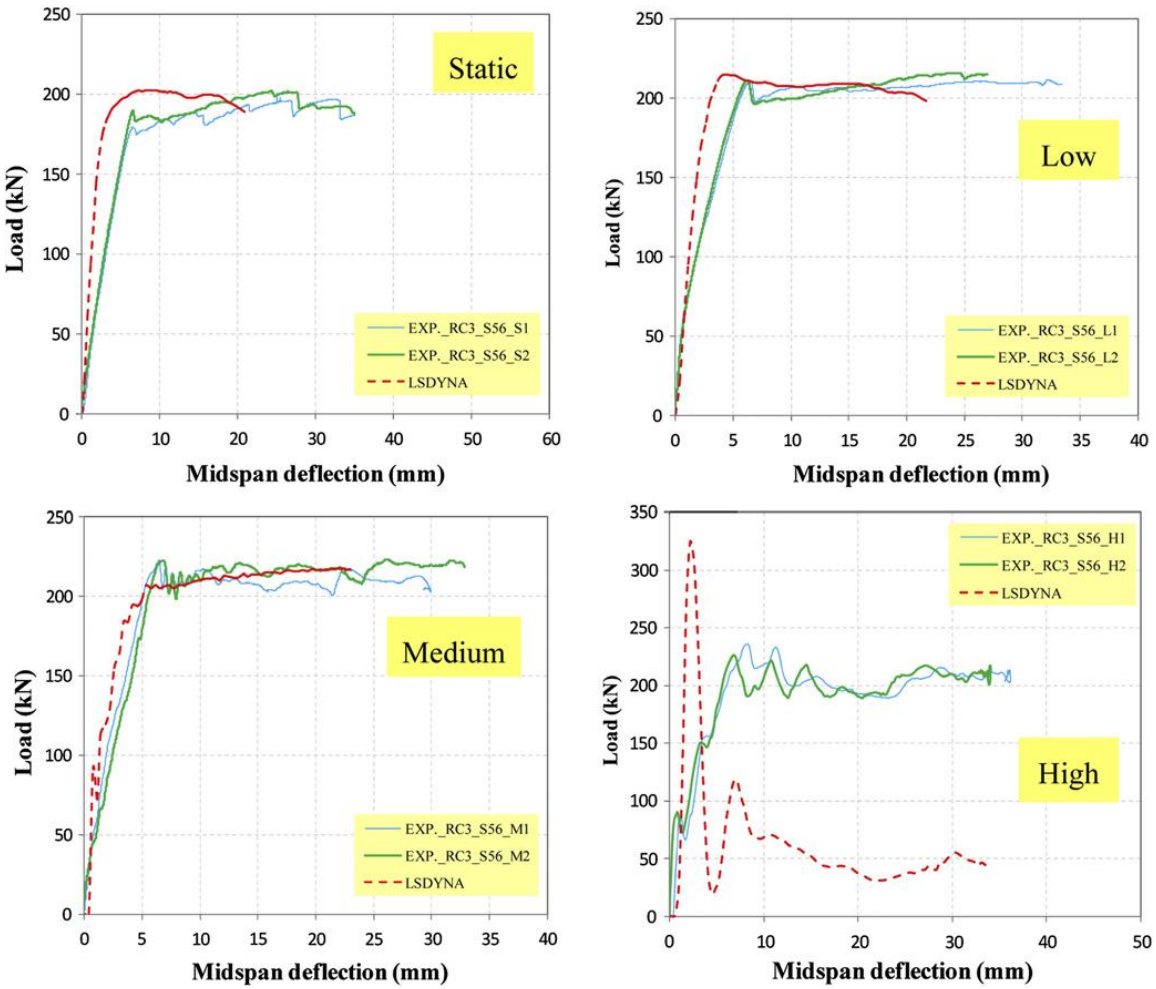
Static
Load (kN)
Midspan deflection (mm)
EXP._RC3_S56_S1
EXP._RC3_S56_S2
LSDYNA
Low
EXP._RC3_S56_L1
EXP._RC3_S56_L2
LSDYNA
Medium
EXP._RC3_S56_M1
EXP._RC3_S56_M2
LSDYNA
High
EXP._RC3_S56_H1
EXP._RC3_S56_H2
LSDYNA

Fig. 13

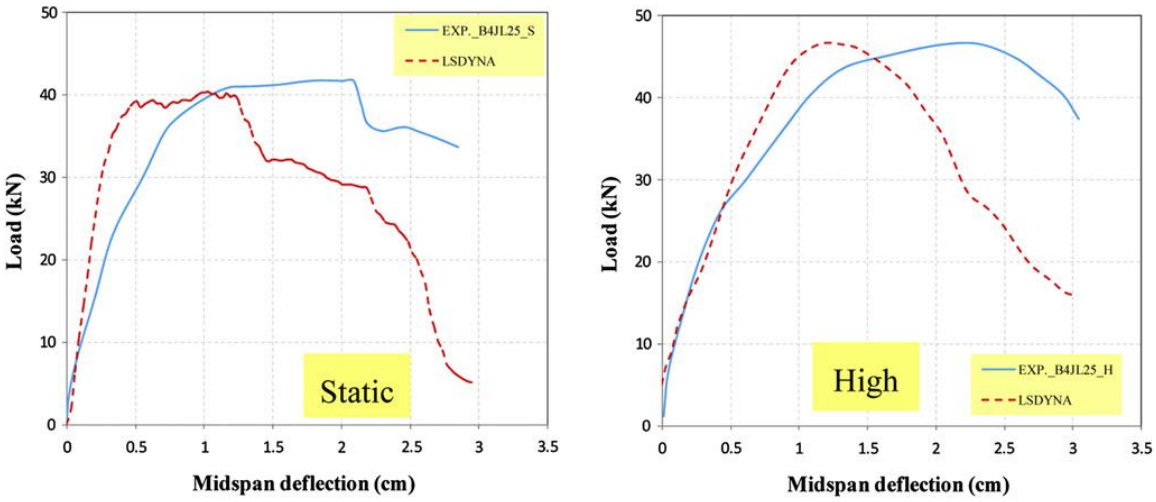
EXP._B4JL25_S
LSDYNA
Static
Load (kN)
Midspan deflection (cm)
EXP._B4JL25_H
LSDYNA
High
Load (kN)
Midspan deflection (cm)

Fig. 14

RC3_S0 RC3_S12 RC3_S56

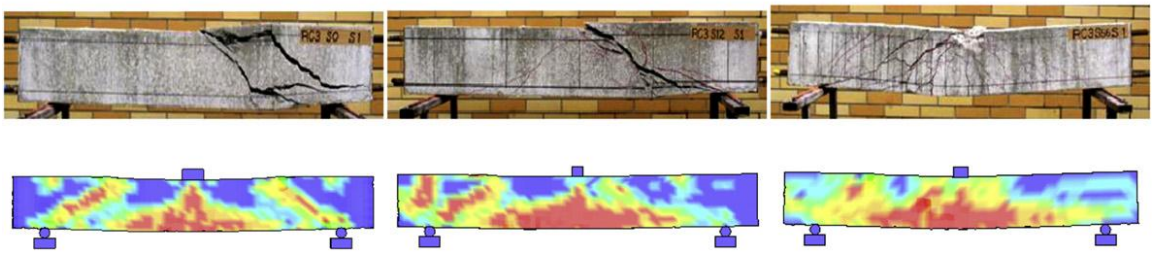

Static

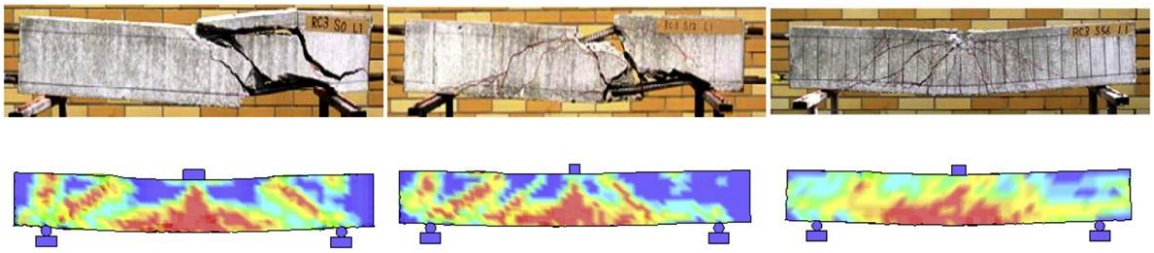

Low

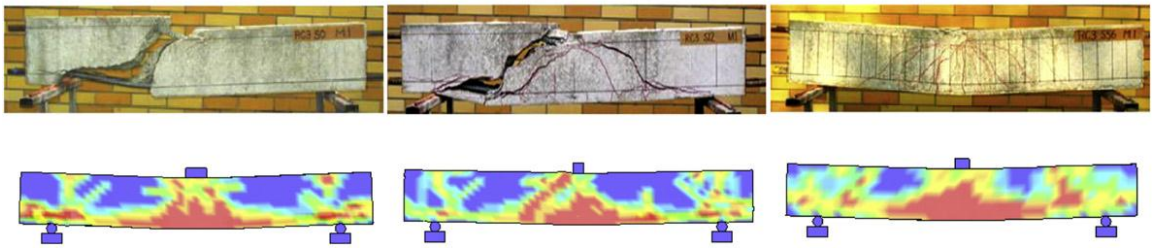

Medium

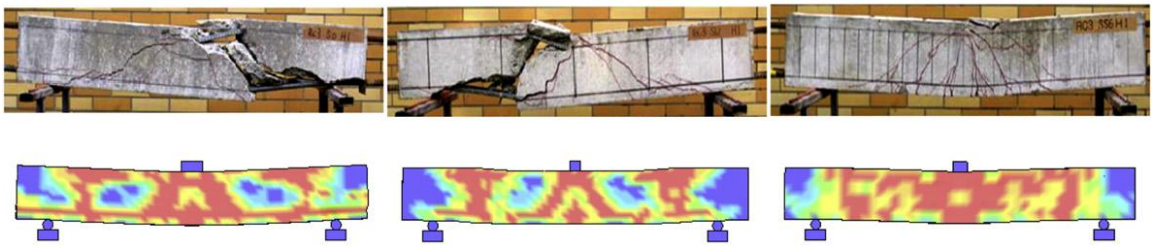

High

Fig. 15

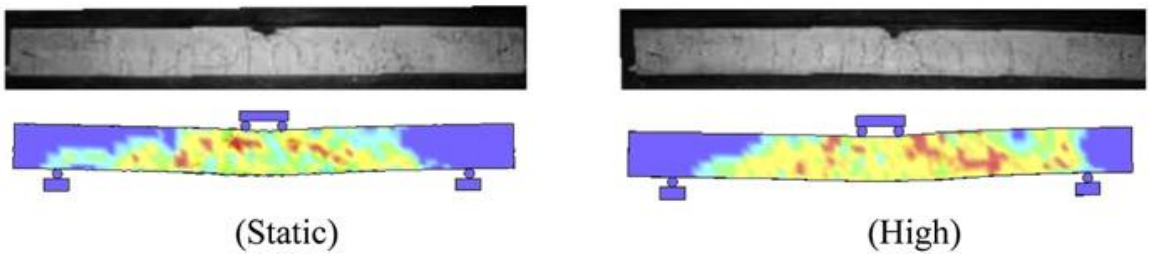

Fig. 16

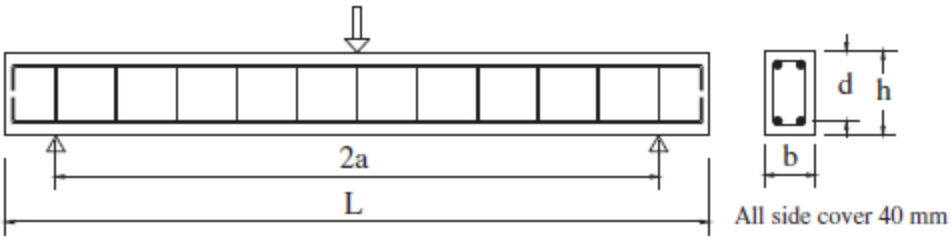

Fig. 17

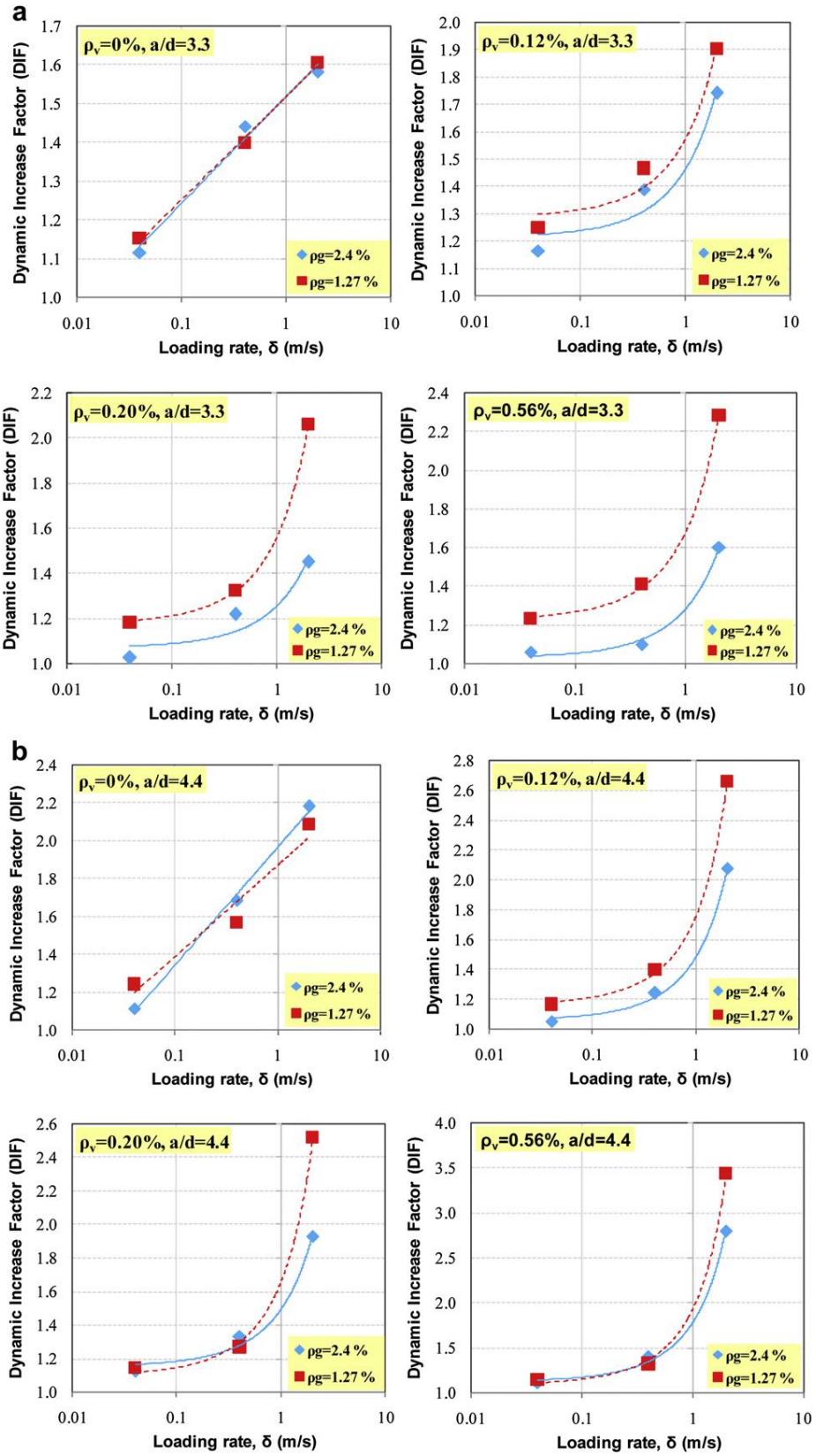
a
ρ_v=0%, a/d=3.3
ρ_v=0.12%, a/d=3.3
ρ_v=0.20%, a/d=3.3
ρ_v=0.56%, a/d=3.3
b
ρ_v=0%, a/d=4.4
ρ_v=0.12%, a/d=4.4
ρ_v=0.20%, a/d=4.4
ρ_v=0.56%, a/d=4.4
Dynamic Increase Factor (DIF)
Loading rate, δ (m/s)
ρg=2.4 %
ρg=1.27 %

Fig. 18

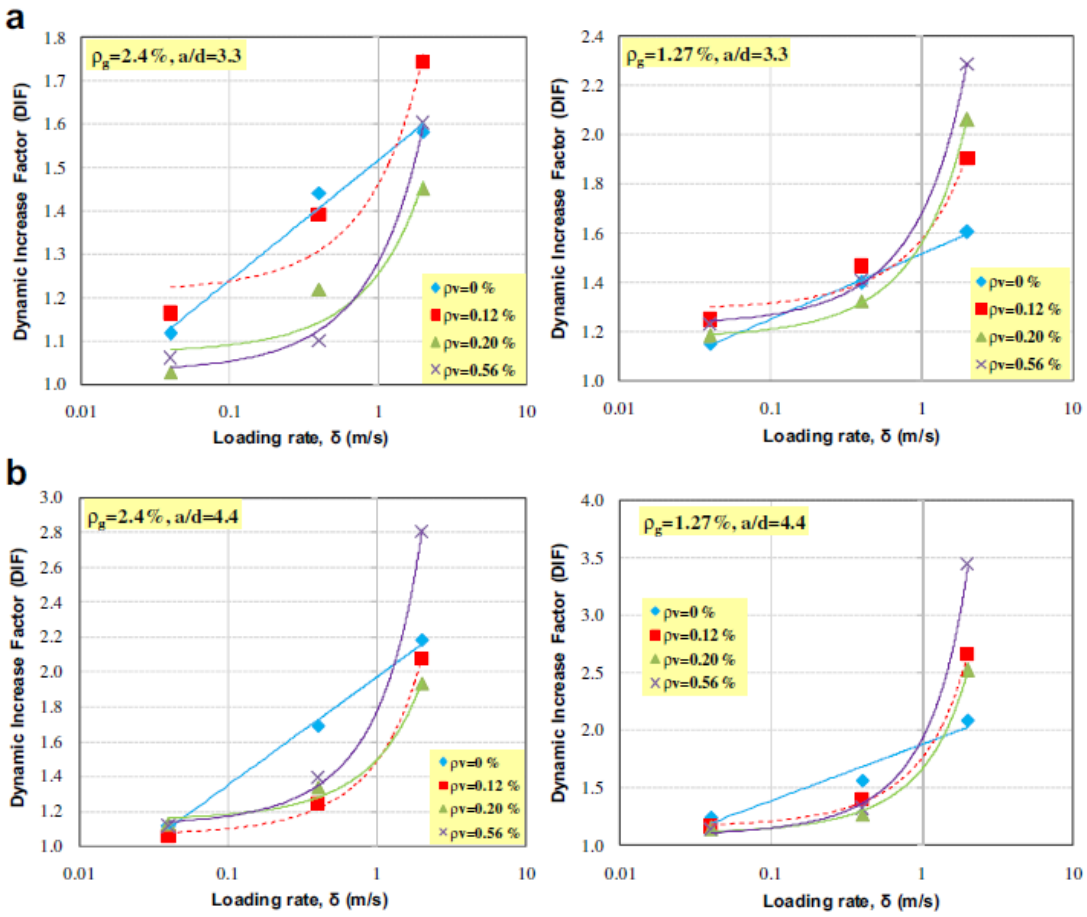
a
ρ_g=2.4 %, a/d=3.3
ρ_g=1.27 %, a/d=3.3
b
ρ_g=2.4 %, a/d=4.4
ρ_g=1.27 %, a/d=4.4
ρv=0 %
ρv=0.12 %
ρv=0.20 %
ρv=0.56 %
Dynamic Increase Factor (DIF)
Loading rate, δ (m/s)

Fig. 19

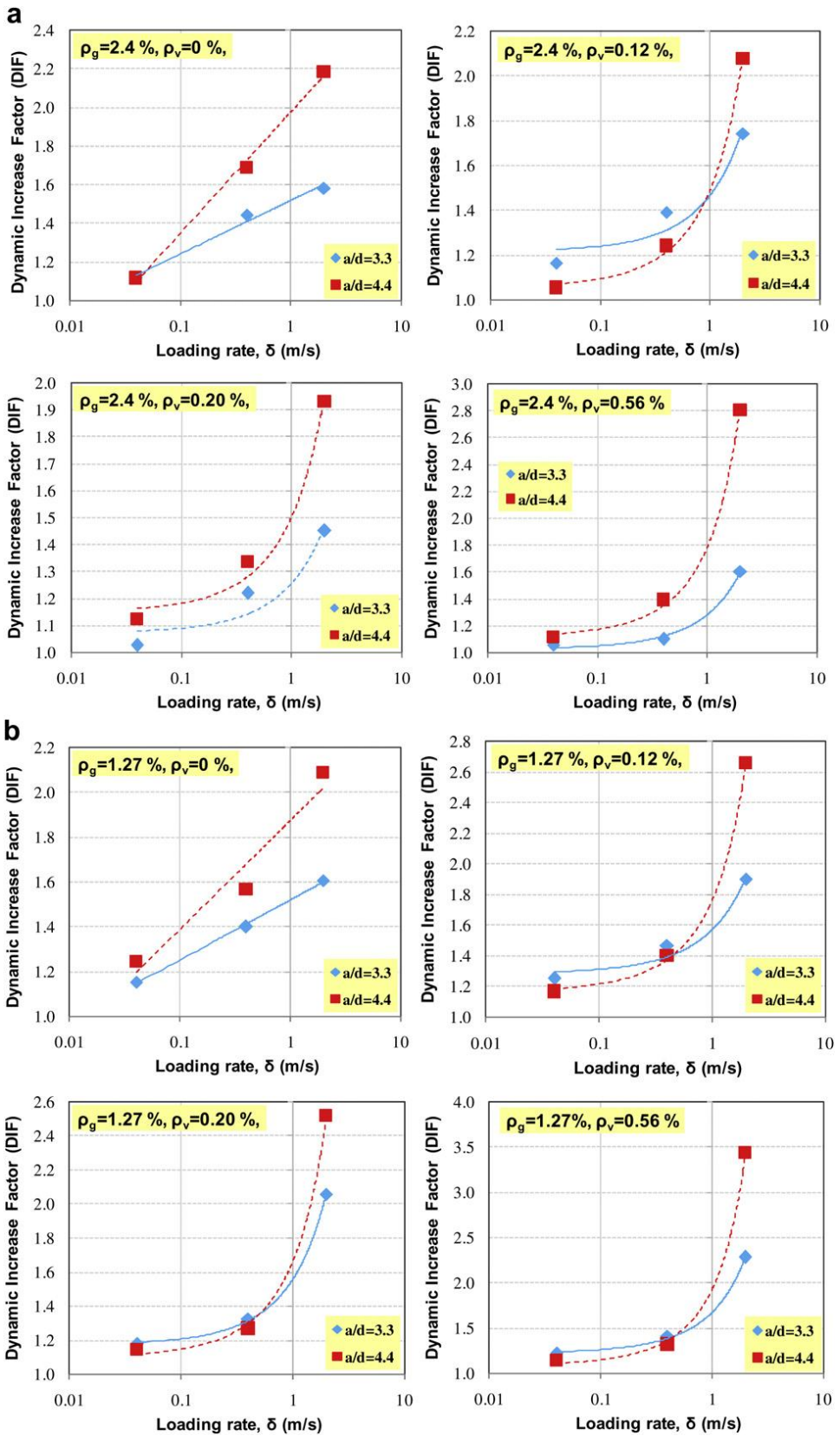
a
ρg=2.4 %, ρv=0 %,
ρg=2.4 %, ρv=0.12 %,
ρg=2.4 %, ρv=0.20 %,
ρg=2.4 %, ρv=0.56 %
b
ρg=1.27 %, ρv=0 %,
ρg=1.27 %, ρv=0.12 %,
ρg=1.27 %, ρv=0.20 %,
ρg=1.27%, ρv=0.56 %
Dynamic Increase Factor (DIF)
Loading rate, δ (m/s)
a/d=3.3
a/d=4.4

Fig. 20

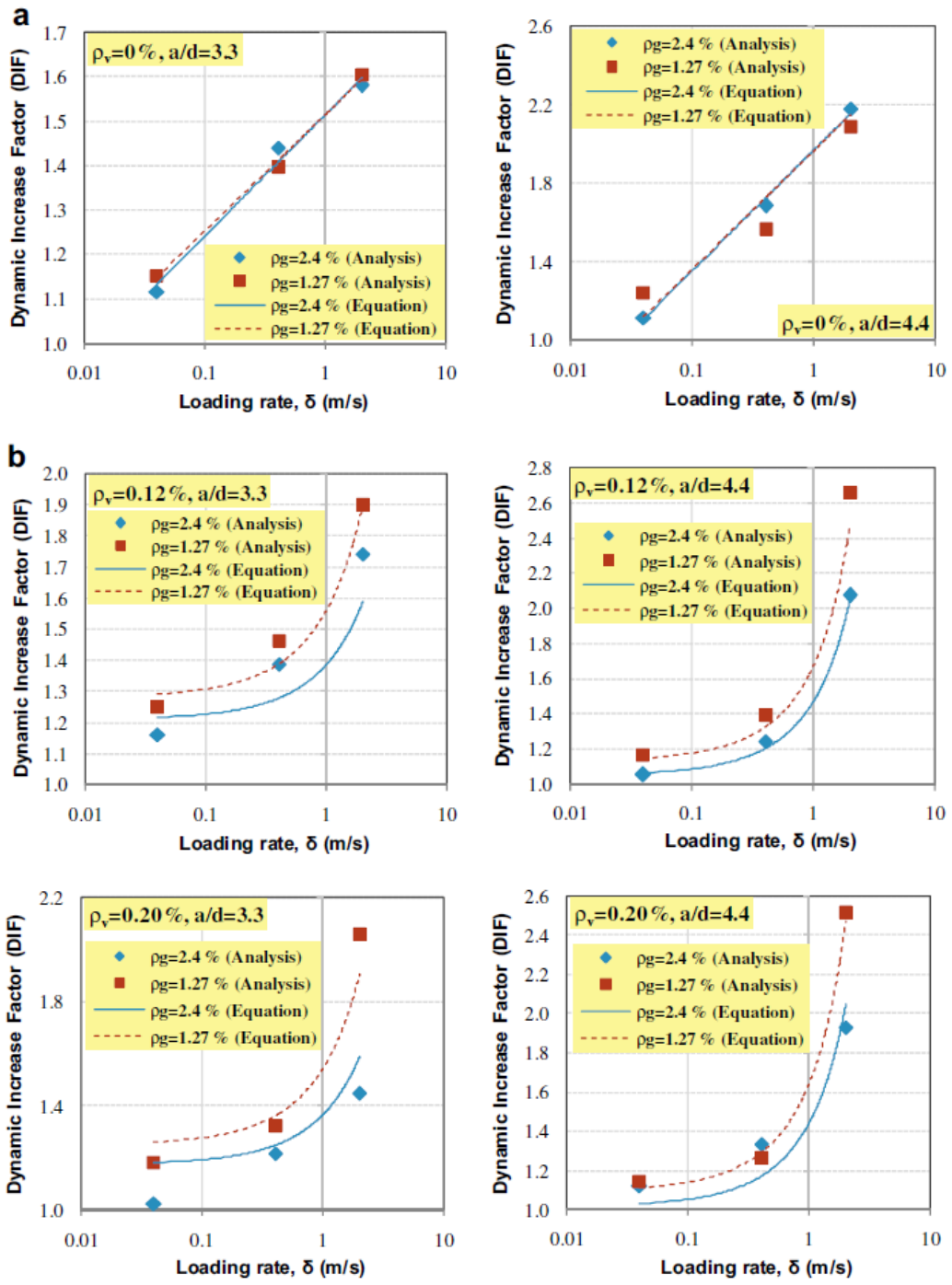
a
ρv=0 %, a/d=3.3
ρg=2.4 % (Analysis)
ρg=1.27 % (Analysis)
ρg=2.4 % (Equation)
ρg=1.27 % (Equation)
Dynamic Increase Factor (DIF)
Loading rate, δ (m/s)
ρv=0 %, a/d=4.4
b
ρv=0.12 %, a/d=3.3
ρv=0.12 %, a/d=4.4
ρv=0.20 %, a/d=3.3
ρv=0.20 %, a/d=4.4

Fig. 21